THE UNIVERSITY OF CHICAGO

Committee on Medical Physics

Propagation-Based X-Ray Phase Contrast Computed Tomography with the Multislice Approximation and Automatic Differentiation

Andrew Ferretti, Giavanna Jadick, Cailey Riggs, and Patrick La Riviere

Department of Radiology, University of Chicago, Chicago, IL, USA

Background

- Propagation-based X-ray phase contrast CT (PB XPC-CT) is a developing imaging modality that seeks to reconstruct the index of refraction of a sample, instead of the typical attenuation coefficients values that may be obtained from conventional X-ray CT [1].
- PB XPC-CT is most applicable to breast imaging, as phase information can provide increased contrast in many weakly absorptive structures, but requires very small detector sizes and specialized sources [2].
- Reconstructions for PB-XPCT typically rely on a number of limiting approximations to make the reconstruction computationally simple.
- New computational advances allow for more complex models, which may increase the quality of the achieved reconstructions [1].
- Complex models also present new challenges, like the lack of an analytic inverse and increased computational demands.

Purpose

- We use simulations to compare iterative PB XPC-CT reconstructions using two forward models to investigate possible improvements in the reconstructed images
- We highlight the use of automatic differentiation in enabling more physically realistic forward modeling

Materials

Phantom and Simulation

For x-ray frequencies, the energy-dependent complex index of refraction is described by

$$n_\omega = 1 - \delta_\omega + i\beta_\omega, \quad (1)$$

where δ_ω is the phase shifting component, and β_ω is related to the linear attenuation coefficient. A voxelized phantom consisting of two bone spheres of different radii placed in a solid tissue cylinder was constructed, consisting of $64\times30\times30$ voxels, with three different voxel sizes of 0.5 µm, 0.25 µm, and 0.1 µm modeled and corresponding phantom thicknesses 32 µm, 16 µm, and 6.4 µm, respectively. The δ_ω and β_ω values for tissue and bone were calculated at 10 keV, modeling a synchrotron experiment. Figure 1 shows the distributions of δ_ω and β_ω for center slice of the resulting phantom.

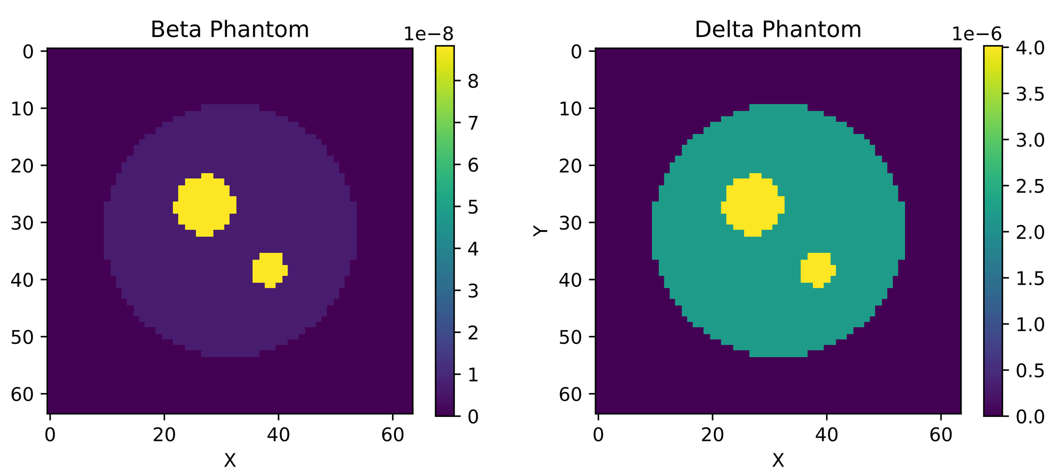

Figure 1. Phantom beta (left) and delta (right) distributions. The phantom consists of two spheres of bone in a cylinder of tissue

Methods

Iterative Reconstruction and Automatic Differentiation

The PB XPC-CT inverse problem can be formulated as a minimization problem, namely,

$$\hat{x} = \underset{\mathbf{x}}{\text{argmin}}\left(||y - f(\mathbf{x})||_2^2 + \vec{\gamma}\cdot\vec{r}(\mathbf{x})\right), \quad (2)$$

where y is a set of PB XPC-CT measurements, $f(\mathbf{x})$ is the predicted set of measurements generated by one of the examined forward models (described in next section) given the current best guess of $\mathbf{x}$, the array of refractive indexes of the sample being imaged, $\vec{r}(\mathbf{x})$ is a total variation (TV) regularization with separate terms for δ_ω and β_ω, and $\vec{\gamma}$ is a set of arbitrary weights setting the strength of the TV penalties [3]. All forward models were implemented in Chromatix, while the minimization of equation 2 was performed using gradient descent in Optax, which natively includes automatic differentiation, enabling the quick calculation of gradients to floating point precision. The weights $\vec{\gamma}$ on the TV term were tuned for each forward model using a parameter search.

Methods Cont.

Forward Models

In general, a forward model in Equation 2 must solve the wave equation in matter (in the region of the sample being probed) and in air (free space propagation to the detector). Under the paraxial assumption, the latter is well described by the Fresnel diffraction operator, which uses the Fourier transform $\mathcal{F}$ to express the complex scalar wave field as

$$\psi(x,y,\Delta) = e^{ik\Delta}\mathcal{F}^{-1}\left\{\exp\left[\frac{-i\Delta(k_x^2+k_y^2)}{2k}\right]\mathcal{F}\{\psi(x,y,0)\}\right\}, \quad (3)$$

where k is the magnitude of the wavevector and k_x and k_y are its x and y components. In the region of the sample, we study two models, the projection approximation (PA) and the multislice approximation (MA) (also shown schematically in Figure 2).

Projection Approximation

- The PA treats the sample like a perturbing screen, with a simple attenuation and phase shifting effect.
- Refractive/self-interference effects inside the sample are ignored.
- Explicitly, $\tilde{\psi}_\omega(x,y,z_0) \approx \exp\left[-ik\int_0^{z_0}(\delta_\omega(\vec{r}) - i\beta_\omega(\vec{r}))\,dz\right]\tilde{\psi}_\omega(x,y,0)$.
- It is valid for large Fresnel numbers $N_F >> 1$, $N_F = \frac{a^2}{\lambda z_0}$, where λ is the wavelength of the incident X-ray field, a is the feature size, and z_0 is the phantom width [1].
- N_F=63, 32, and 13 for the feature sizes in this work.

Multislice Approximation

- The MA divides a sample into sections in which the PA is valid, and then performs a projection and free-space propagation in each slice.
- This allows refractive effects in the sample to be considered.

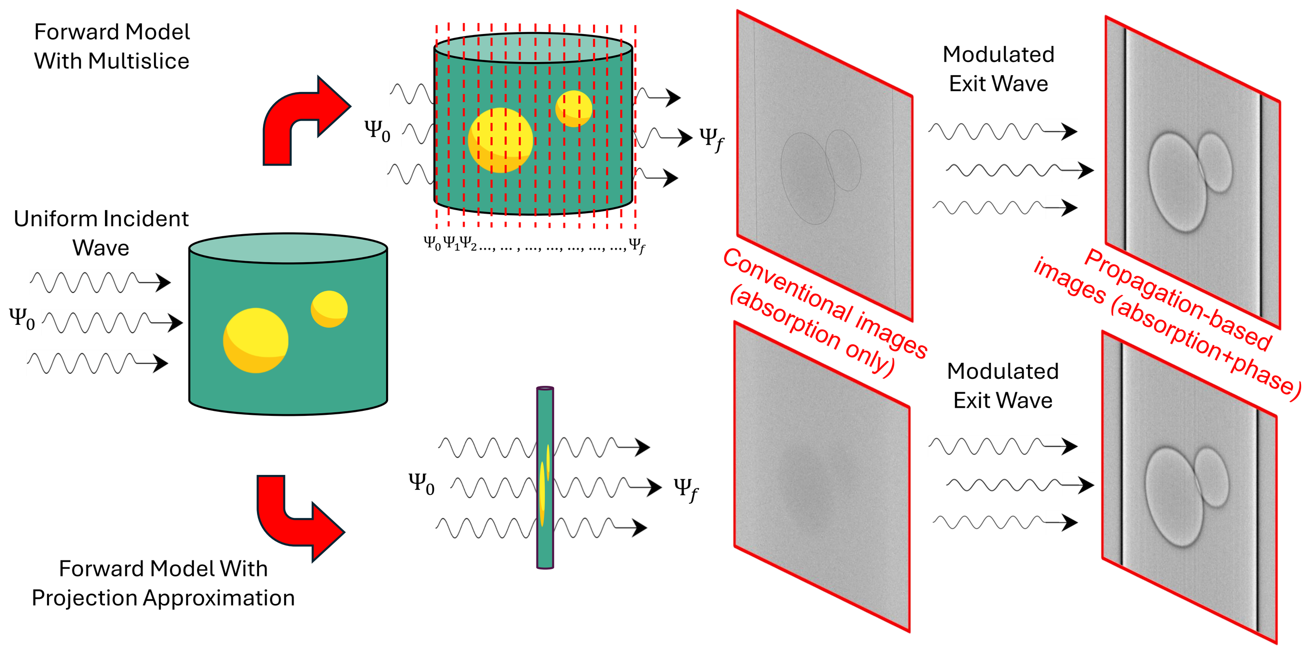

Figure 2. Schematic of the the PA and MA Forward Models

Image Assessment

Reconstructions using the MA and PA at low and high noise levels were compared using four metrics

- Total RMSE, $RMSE_{\text{total}} = \sqrt{\frac{1}{N}\sum_{n=1}^{N}(\mathbf{x}_{recon} - \mathbf{x}_{exact})^2}$
- Delta Image RMSE, $RMSE_\delta = \sqrt{\frac{1}{N}\sum_{n=1}^{N}((\delta_\omega(\vec{r}))_{recon} - (\delta_\omega(\vec{r}))_{exact})^2}$
- Beta Image RMSE, $RMSE_\beta = \sqrt{\frac{1}{N}\sum_{n=1}^{N}((\beta_\omega(\vec{r}))_{recon} - (\beta_\omega(\vec{r}))_{exact})^2}$
- Delta Image SNR, $SNR_\delta = \mu_{bone} - \mu_{tissue}/\sqrt{\frac{1}{2}\sigma_{bone}^2 + \frac{1}{2}\sigma_{tissue}^2}$
- Beta Image SNR, $SNR_\beta = \mu_{bone} - \mu_{tissue}/\sqrt{\frac{1}{2}\sigma_{bone}^2 + \frac{1}{2}\sigma_{tissue}^2}$

Results

Pixel Size	0.5				0.25				0.1			
Noise	Low		High		Low		High		Low		High	
Forward Model	MS	PA	MS	PA	MS	PA	MS	PA	MS	PA	MS	PA
$RMSE_{\text{total}}$ $(\times10^{-8})$	1.2	2.4	3.4	6.6	0.3	1.8	3.5	3.8	1.0	2.0	5.2	6.7
$RMSE_\delta$ $(\times10^{-8})$	1.7	3.3	4.8	9.3	0.4	2.5	4.8	5.3	1.5	2.8	7.3	9.4
$RMSE_\beta$ $(\times10^{-8})$	0.3	0.5	0.6	0.7	0.2	0.6	0.8	0.8	0.3	0.5	1.0	1.0
δ_ω SNR	53	26	31	24	151	36	15	14	24	15	5.6	4.7
β_ω SNR	9.6	3.8	-	-	23	5.8	-	-	5.7	3.0	-	-

Table 1. Image quality metrics at all pixel sizes, two noise levels, and PA and MA forward models

Results Cont.

Table 1 provides the RMSEs and SNRs for all noise, pixel size, and forward model combinations, while Figures 3 and 4 show the corresponding δ_ω and β_ω reconstructions at the center slice. At all feature sizes, relative to PA, MA gave phase images with lower $RMSE_{total}$ values, $RMSE_\delta$ values, and higher SNR_δ values (although the difference in SNR decreases at high noise). Geometrically accurate attenuation reconstructions were only obtainable at low noise, where MA likewise produced images with lower $RMSE_\beta$ values and higher SNR_β values.

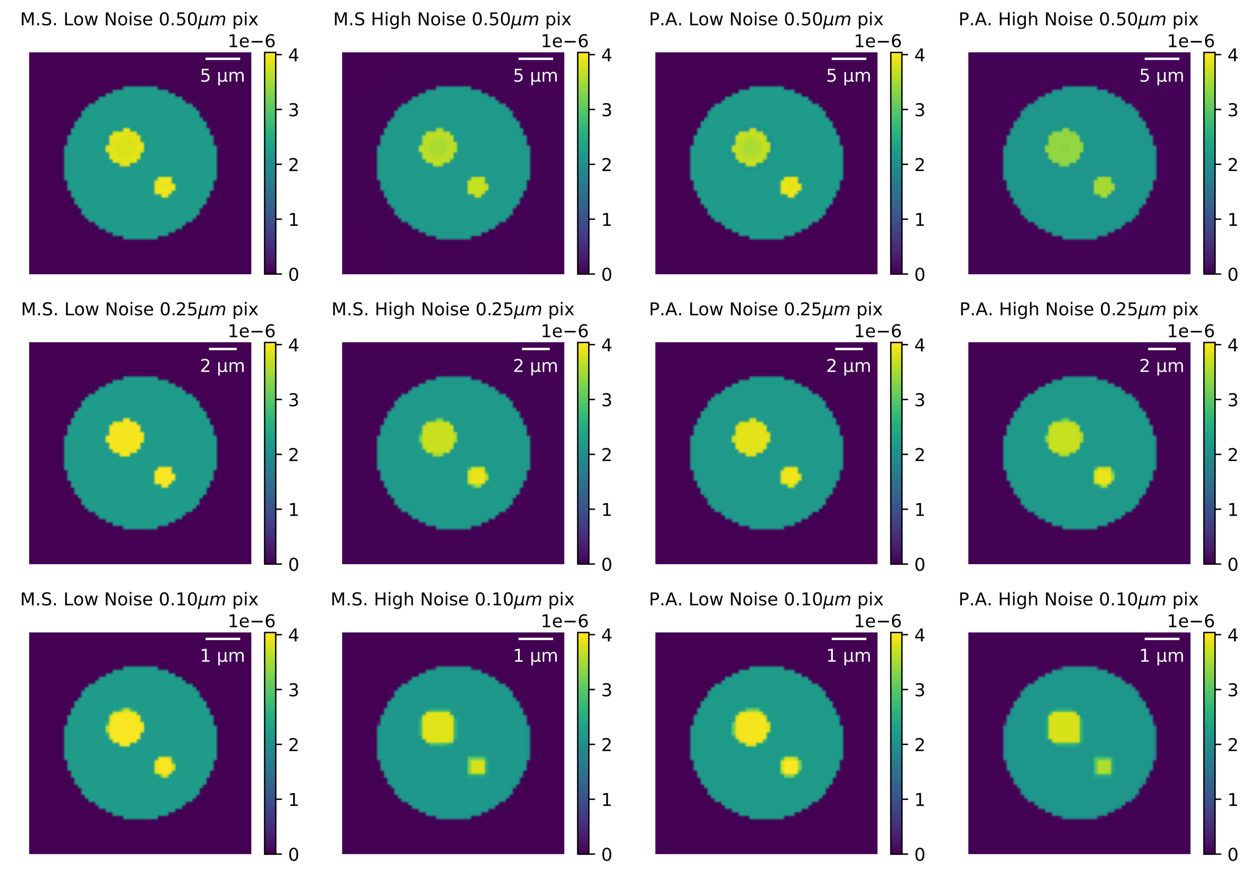

Figure 3. Delta reconstructions at all noise and pixel combinations

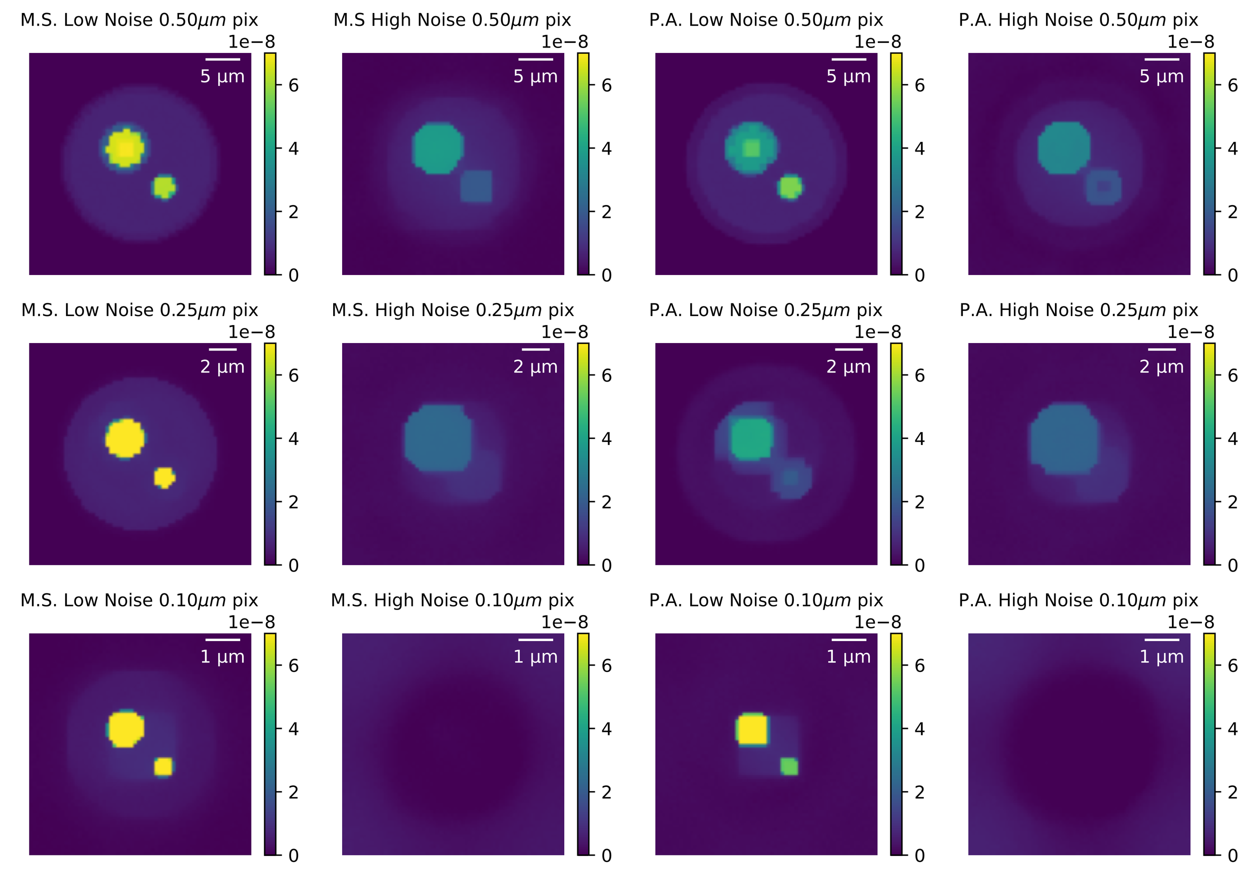

Figure 4. Beta reconstructions at all noise and pixel combinations

Conclusions

- Using the multislice approximation in iterative reconstruction of PB XPC-CT data results in a measurable improvement in image quality against the projection approximation in the regime of voxel sizes explored.
- The MA and PA are also comparable in some regimes, so the PA may be preferable at times as the MA still has a higher computational cost associated it.
- Future work should include verifying these results over a broad range of pixel sizes and x-ray energies.

References

[1] D. Paganin and D. Pelliccia, “X-ray phase contrast imaging: a broad overview of some fundamentals,” in Advances in Imaging and Electron Physics, vol. 218, Amsterdam, Netherlands: Academic Press, 2016, pp. 64–148

[2] Y. Zhao et al., “High-resolution, low-dose phase contrast X-ray tomography for 3D diagnosis of human breast cancers,” Proceedings of the National Academy of Sciences, vol. 109, no. 45, pp. 18290–18294, Sep. 2012. doi:10.1073/pnas.1204460109

[3] B. De Man and J. Fessler, “Statistical Iterative Reconstruction for X-Ray Computed Tomography,” in Biomedical Mathematics: Promising Directions in Imaging, Therapy Planning, and Inverse Problems, Medical Physics Publishing, 2010

aeferretti@uchicago.edu